Construction of glutinous rice potpourri-like Mott−Schottky Ni/CeO_2 heterojunction nanosheets for robust electrochemical water reduction

Guangqiang Zhang[#], *Hong Su*[#], *Yan Zhang**

Guangqiang Zhang and Hong Su equally contribute to this work.

Sichuan Engineering Research Center for Biomimetic Synthesis of Natural Drugs,

School of Life Science and Engineering, Southwest Jiaotong University, Chengdu, Sichuan

610031, China

E-mail: zyzw@swjtu.edu.cn

Experimental Section

Materials and Chemicals

Pyromellitic acid hydrate ($C_{10}H_6O_8$, >98% Aladdin), cerium nitrate hexahydrate ($Ce(NO_3)_3 \cdot 6H_2O$, 99,2% Aladdin), The Nickel (II) acetate ($Ni(CH_3COO)_2 \cdot 4H_2O$, 99.2%), Urea ($CH_4N_2O$, 98%) and Nafion (5 wt%) were purchased from Shanghai Macklin Biochemical Company. Pt/C (10 wt %) was purchased from bidepharm. Deionized water used throughout all experiments was purified through a Millipore system.

All chemicals and reagents were used as received without further purification.

Synthesis of Ce-based coordination polymer NSs

$Ce(NO_3)_3 \cdot 6H_2O$ (434.0 mg), Pyromellitic acid hydrate (254.0 mg) were dissolved into 20 mL ethanol with magnetic stirring for 10 min to obtain a homogeneous solution. Subsequently, the mixture was transferred into a 50 mL Teflon-lined stainless steel autoclave and heated at 80 °C for 1 h. Finally, after the autoclave cooled down to room temperature, the resulting precursor was successively washed with deionized water and ethanol several times, and then dried overnight in an oven at 60 °C.

Synthesis of NiO/CeO2 NSs

The as-prepared Ce-based coordination polymer precursor was uniformly mixed with $Ni(CH_3COO)_2 \cdot 4H_2O$ at a mass ratio of 1:3. Subsequently, the mixture was annealed in air at 600 °C for 120 min to obtain NiO/CeO_2 NSs.

Synthesis of Ni/CeO2 HJ-NSs

A glutinous rice potpourri-like Ni/CeO_2 HJ-NSs via a scalable urea reduction reaction. Briefly, the corresponding precursor and urea were separately placed in two quartz tubes which were concatenated. The urea was placed on an alumina boat in the lower temperature region of the tube furnace and the NiO/CeO_2 NSs were placed in an upside down position on another alumina boat at the center and heated to 800 °C for 1 h with a ramping rate of 10 °C min^{-1} under Ar atmosphere. Through the reduction selectivity of urea, NiO was specifically reduced to metallic Ni and CeO_2 did not change. After naturally cooling to ambient temperature, the black powder product was successfully obtained.

In addition, CeO_2 were fabricated under the same experimental conditions except without the involvement of nickel precursors.

Materials characterization

The obtained sample was characterized by a field-emission scanning electron microscope (SEM, FEI Inspect F50) coupled with an energy dispersive spectrometer (EDS) analyzer, a transmission electron microscope (TEM, FEI Tecnai G2 Spirit TWIN). The phase and composition of the sample were analyzed by a X-ray diffractometer with Cu K_α (λ = 1.5406 Å) radiation (XRD, PANalytical B.V.). X-ray photoelectron spectroscopy (XPS, Thermo Scientific Escalab 250xi) was employed to analyze the valence state of the element on the surface of samples. Nitrogen absorption/desorption analysis was carried out on a BET surface-area and pore-size analyzer (Micromeritics ASPA 2020) to acquire the specific surface area and pore size distribution.

Electrochemical Measurements

The electrochemical test was accomplished on a CS150H Electrochemical Workstation using a typical three-electrode configuration. An iR-correction was used for all the electrochemical tests. A carbon cloth (CC) electrode was used as the working electrode, a graphite rod was used as a counter electrode and saturated calomel electrode (SCE) was used as a reference electrode. To prepare the

working electrode, 6.0 mg of the catalyst were ultrasonically dispersed for 20 min in a mixture solvent containing 300 μL ethanol and 100.0 μL Nafion (5 wt%) solution. Afterward, 50 μL of the above suspension was dropped onto the CC electrode (loading amount: 1 mg cm^{-2}) and then dried at room temperature. The electrochemical measurements were executed in 1 M KOH electrolyte. All potentials were converted to a reversible hydrogen electrode (RHE) based on the following equation: $E_{RHE}=E_{SCE} + 0.0592pH + 0.241$. The linear sweep voltammetry (LSV) curves for HER were recorded in the potential range of -0.73 - 0.07 V (vs. RHE) with a scan rate of 5 mV s^{-1}. The chronopotentiometric measurements for HER were performed at a constant current density of 10 mA cm^{-2} for up to 50 h. The cycle voltammetry (CV) curves for HER were recorded in the potential range of 1.10 - 1.20 V (vs. RHE) at different scan rates (from 20 to 120 mV s^{-1}) to evaluate the active surface area of the catalyst. Electrochemical impedance spectra (EIS) were tested at the applied potential corresponding to the potential of -0.72 V (vs. RHE) for HER within frequency window ranging from 100 kHz to 0.01 Hz.

Calculation of Electrochemical active surface area (ECSA) for each catalyst

In order to obtain the ECSA of the working electrode, the specific capacitance of the flat surface is usually in the range of 20-60 μF cm^{-2}, we choose the median value of 40 μF cm^{-2} as the calculation standard. The roughness factor (R_f) is first obtained according to the equation: $R_f=C_{dl}/40$ μF cm^{-2}. The electrochemically active surface area is directly obtained by the equation: $ECSA=R_f S$, where S is usually equal to the geometrical area of the electrode (here S=0.5 cm^2).

Calculation of Turnover frequency (TOF) for each catalyst

The TOF value is calculated according to the following formula:

$$\mathrm{TOF} = \frac{\mathrm{ImFA}}{4\mathrm{RT}\cdot\mathrm{slope}}$$

Where I is the current during the linear sweep voltammetry test (the unit is A). m represents the electro transfer numbers in HER and OER, which are 2 and 4 respectively. F is Faraday's constant (the unit is C mol^{-1}) and A is the geometric area of the electrode (0.5 cm^2). R is the gas constant and T is absolute temperature. slope is the linear relationship between the oxidation peak and the scanning rate in electrochemical cyclic voltammetry.

Supplementary Figures and Tables

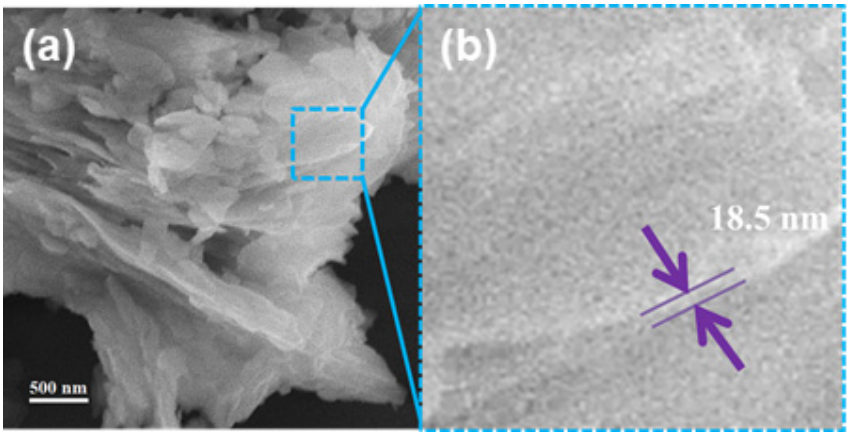

Figure S1. (a) SEM image of Ce-based coordination polymer. (b) Enlarged a cross-section image of light blue dotted box in (a).

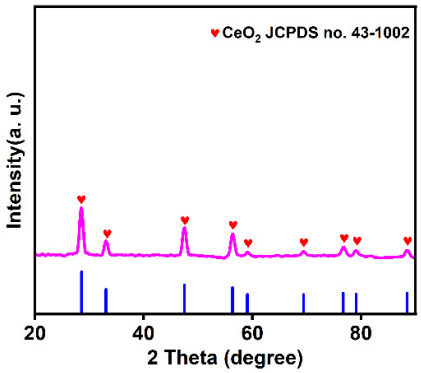

Figure S2. XRD pattern of CeO_2 NSs.

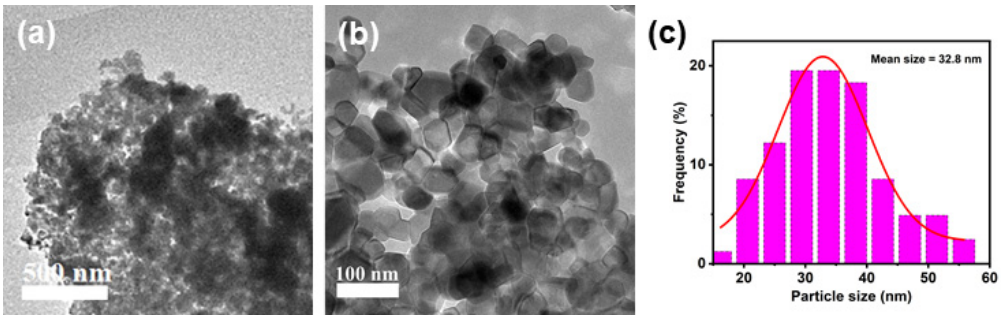

Figure S3. (a) TEM image, (b) enlarged TEM image, and (c) particle size distribution of Ni/CeO_2.

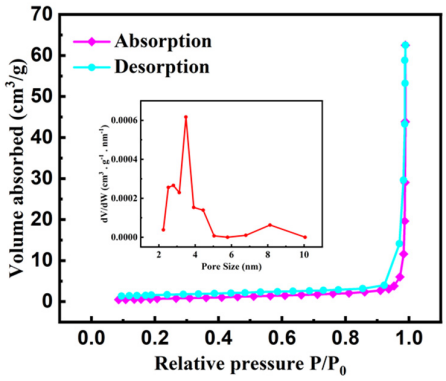

Figure S4. Nitrogen adsorption-desorption isotherms of Ni/CeO_2 HJ-NSs, pore size distribution (inset of S4).

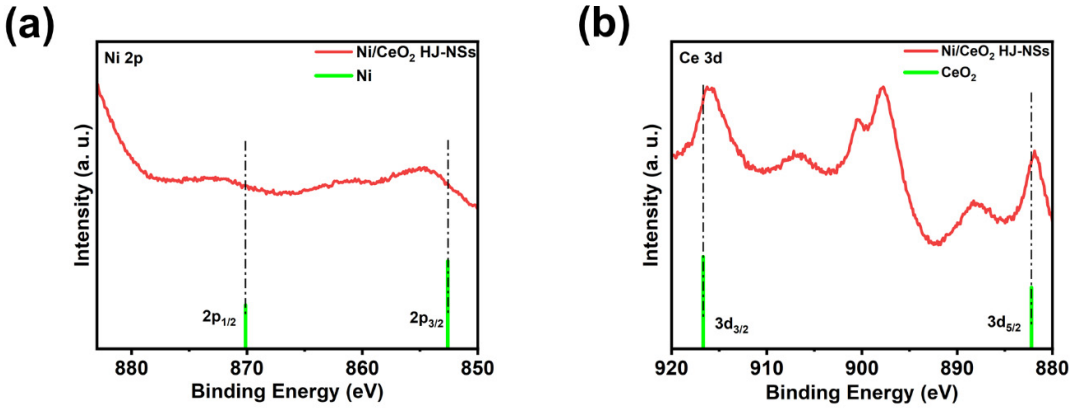

Figure S5. Comparisons of the (a) Ni 2p and (b) Ce 3d XPS spectra for different catalysts.

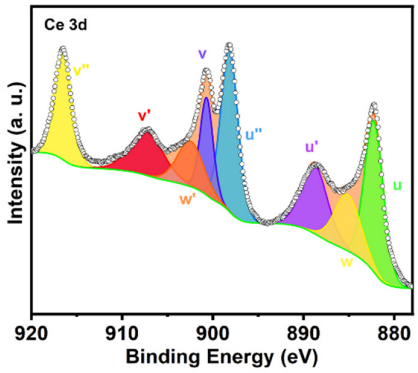

Figure S6. Deconvoluted Ce 3d XPS spectra for pure CeO_2 catalysts.

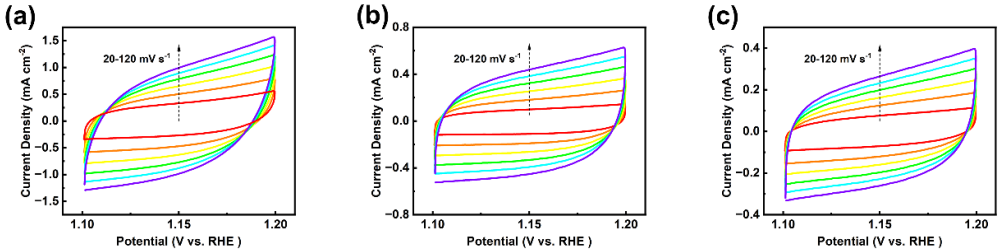

Figure S7. CV curves of different samples in the non-Faradaic region (1.10-1.20 V (vs. RHE)) obtained at different scanning rates. (a) Ni/CeO_2 HJ-NSs, (b) NiO/CeO_2 NSs, and (c) CeO_2 NSs.

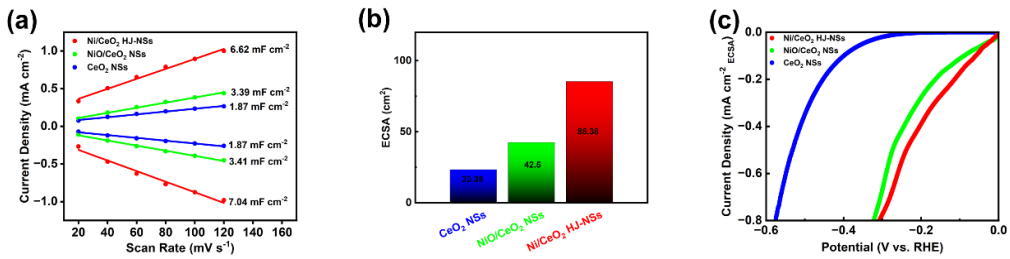

Figure S8. (a) The Cdl, (b) corresponding ECSA, and (c) HER polarization curves with the current density normalized by ECSA of Ni/CeO_2 HJ-NSs, NiO/CeO_2 NSs and CeO_2 NSs.

Calculation of ECSA for each catalyst:

$$A_{ECSA}^{CeO_2} = \frac{1870\ \mu F\ cm^{-2} x\ 0.5 cm^2}{40\ \mu F\ cm^{-2}\ per\ cm^2_{ECSA}} = 23.38\ \ cm^2_{ECSA}$$

$$A_{ECSA}^{NiO/CeO_2} = \frac{3400\ \mu F\ cm^{-2}\ x\ 0.5 cm^2}{40\ \mu F\ cm^{-2}\ per\ cm^2_{ECSA}} = 42.5\ \ cm^2_{ECSA}$$

$$A_{ECSA}^{Ni/CeO_2} = \frac{6830\ \mu F\ cm^{-2}\ x\ 0.5 cm^2}{40\ \mu F\ cm^{-2}\ per\ cm^2_{ECSA}} = 85.38\ \ cm^2_{ECSA}$$

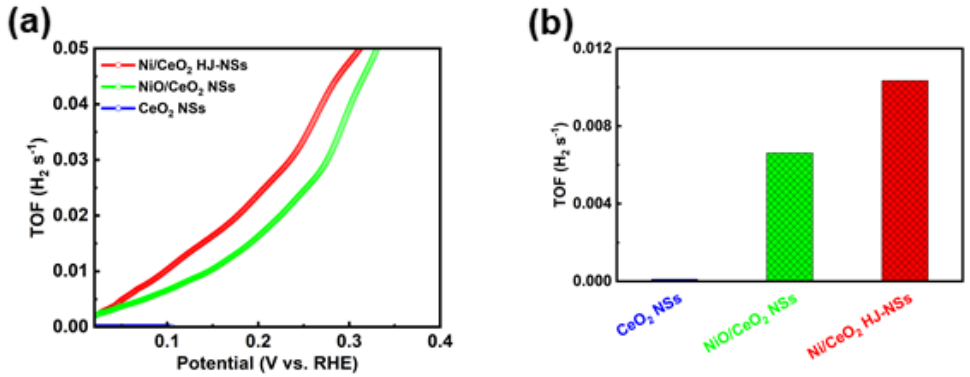

Figure S9. (a) TOF plots for Ni/CeO_2 HJ-NSs, NiO/CeO_2 NSs and CeO_2 NSs. (b) The TOF values at the overpotential of 0.1 V.

Table S1 Elemental analysis of Ni, Ce (measured by ICP-OES) for CeO_2 HJ-NSs catalyst.

Atomic %	Ni	Ce
Ni/CeO_2 HJ-NSs	64.71	11.76

Table S2 Comparison of HER performance in alkaline environment between Ni/CeO_2 HJ-NSs and previously reported representative catalysts.

Electrocatalysts	Overpotentail@ 10 mA cm^{-2} (mV)	Tafel slope (mV dec^{-1})	Electrolyte	Reference
Ni/CeO_2 HJ-NSs	72	65	1.0 M KOH	This work
Pt/C	59	40	1.0 M KOH	This work
OH-Ni/Ni_3C	72	106.3	1.0 M KOH	[1]
Co/Mo_2C@C	98	68	1.0 M KOH	[2]
Cu_3N@CoNiCHs@CF	182	134	1.0 M KOH	[3]
MnCo-CH@NiFe-OH	177	97.8	1.0 M KOH	[4]
Co_9S_8 /Cu_2S/CF	165	80.2	1.0 M KOH	[5]
0.02 Ni–MoP	162	102.6	1.0 M KOH	[6]
Ni-Ni_3C/CC	98	88.5	1.0 M KOH	[7]
MoS_2/Co_9S_8/Ni_3S_2/Ni	113	85	1.0 M KOH	[8]
Ni-doped graphitic carbon	220	64	1.0 M KOH	[9]
Mo_2C/N-PC	100	94.5	1.0 M KOH	[10]
CoP/NiCoP NTs	133	87	1.0 M KOH	[11]
MoP/Mo_2N	89	78	1.0 M KOH	[12]
Ni/NiCoP NHs	90	95	1.0 M KOH	[13]
Co-Ni_3N/CC	194	156	1.0 M KOH	[14]
Ni_{SA}-MoS_2/CC	98	75	1.0 M KOH	[15]
CeO_2/Ni-TMO	93	69	1.0 M KOH	[16]
N-doped Ni_3S_2	155	113	1.0 M KOH	[17]

Reference

(1) Wen, Q.; Duan, J.; Wang, W.; Huang, D.; Liu, Y.; Shi, Y.; Fang, J.; Nie, A.; Li, H.; Zhai, T. Engineering a Local Free Water Enriched Microenvironment for Surpassing Platinum Hydrogen Evolution Activity. *Angew. Chem. Int. Ed.*, e202206077.

(2) Yuan, S.; Xia, M.; Liu, Z.; Wang, K.; Xiang, L.; Huang, G.; Zhang, J.; Li, N. Dual synergistic effects between Co and Mo_2C in Co/Mo_2C heterostructure for electrocatalytic overall water splitting. *Chem. Eng. J.* **2022**, *430*, 132697.

(3) Liu, S.-Q.; Gao, M.-R.; Liu, S.; Luo, J.-L. Hierarchically assembling cobalt/nickel carbonate hydroxide on copper nitride nanowires for highly efficient water splitting. *Appl. Catal. B* **2021**, *292*, 120148.

(4) Zeng, Y.; Cao, Z.; Liao, J.; Liang, H.; Wei, B.; Xu, X.; Xu, H.; Zheng, J.; Zhu, W.; Cavallo, L.; et al. Construction of hydroxide pn junction for water splitting electrocatalysis. *Appl. Catal. B* **2021**, *292*, 120160.

(5) Zang, Z.; Wang, X.; Li, X.; Zhao, Q.; Li, L.; Yang, X.; Yu, X.; Zhang, X.; Lu, Z. Co_9S_8 Nanosheet Coupled Cu_2S Nanorod Heterostructure as Efficient Catalyst for Overall Water Splitting. *ACS Appl. Mater. Interfaces* **2021**, *13* (8), 9865-9874.

(6) Xiao, W.; Zhang, L.; Bukhvalov, D.; Chen, Z.; Zou, Z.; Shang, L.; Yang, X.; Yan, D.; Han, F.; Zhang, T. Hierarchical ultrathin carbon encapsulating transition metal doped MoP electrocatalysts for efficient and pH-universal hydrogen evolution reaction. *Nano Energy* **2020**, *70*, 104445.

(7) Wang, P.; Qin, R.; Ji, P.; Pu, Z.; Zhu, J.; Lin, C.; Zhao, Y.; Tang, H.; Li, W.; Mu, S. Synergistic Coupling of Ni Nanoparticles with Ni_3C Nanosheets for Highly Efficient Overall Water Splitting. *Small* **2020**, *16* (37), 2001642.

(8) Yang, Y.; Yao, H.; Yu, Z.; Islam, S. M.; He, H.; Yuan, M.; Yue, Y.; Xu, K.; Hao, W.; Sun, G.; et al. Hierarchical Nanoassembly of MoS_2/Co_9S_8/Ni_3S_2/Ni as a Highly Efficient Electrocatalyst for Overall Water Splitting in a Wide pH Range. *J. Am. Chem. Soc.* **2019**, *141* (26), 10417-10430.

(9) Zhou, B.; Zhang, M.; He, W.; Wang, H.; Jian, M.; Zhang, Y. Blue rose-inspired approach towards highly graphitic carbons for efficient electrocatalytic water splitting. *Carbon* **2019**, *150*, 21-26.

(10) Han, W.; Chen, L.; Ma, B.; Wang, J.; Song, W.; Fan, X.; Li, Y.; Zhang, F.; Peng, W. Ultra-small Mo_2C nanodots encapsulated in nitrogen-doped porous carbon for pH-universal hydrogen evolution: insights into the synergistic enhancement of HER activity by nitrogen doping and structural defects. *J. Mater. Chem. A* **2019**, *7* (9), 4734-4743.

(11) Lin, Y.; Sun, K.; Liu, S.; Chen, X.; Cheng, Y.; Cheong, W.-C.; Chen, Z.; Zheng, L.; Zhang, J.; Li, X.; et al. Construction of CoP/NiCoP Nanotadpoles Heterojunction Interface for Wide pH Hydrogen Evolution Electrocatalysis and Supercapacitor. *Adv. Energy Mater.* **2019**, *9* (36), 1901213.

(12) Gu, Y.; Wu, A.; Jiao, Y.; Zheng, H.; Wang, X.; Xie, Y.; Wang, L.; Tian, C.; Fu, H. Two-Dimensional Porous Molybdenum Phosphide/Nitride Heterojunction Nanosheets for pH-Universal Hydrogen Evolution Reaction. *Angew. Chem. Int. Ed.* **2021**, *60* (12), 6673-6681.

(13) Lin, Y.; Pan, Y.; Liu, S.; Sun, K.; Cheng, Y.; Liu, M.; Wang, Z.; Li, X.; Zhang, J. Construction of multi-dimensional core/shell Ni/NiCoP nano-heterojunction for efficient electrocatalytic water splitting. *Appl. Catal. B* **2019**, *259*, 118039.

(14) Zhu, C.; Wang, A.-L.; Xiao, W.; Chao, D.; Zhang, X.; Tiep, N. H.; Chen, S.; Kang, J.; Wang, X.; Ding, J.; et al. In Situ Grown Epitaxial Heterojunction Exhibits High-Performance Electrocatalytic Water Splitting. *Adv. Mater.* **2018**, *30* (13), 1705516.

(15) Wang, Q.; Zhao, Z. L.; Dong, S.; He, D.; Lawrence, M. J.; Han, S.; Cai, C.; Xiang, S.; Rodriguez, P.; Xiang, B.; et al. Design of active nickel single-atom decorated MoS_2 as a pH-universal catalyst for hydrogen evolution reaction. *Nano Energy* **2018**, *53*, 458-467.
(16) Long, X.; Lin, H.; Zhou, D.; An, Y.; Yang, S. Enhancing Full Water-Splitting Performance of Transition Metal Bifunctional Electrocatalysts in Alkaline Solutions by Tailoring CeO_2 –Transition Metal Oxides–Ni Nanointerfaces. *ACS Energy Lett.* **2018**, *3* (2), 290-296.
(17) Kou, T.; Smart, T.; Yao, B.; Chen, I.; Thota, D.; Ping, Y.; Li, Y. Theoretical and Experimental Insight into the Effect of Nitrogen Doping on Hydrogen Evolution Activity of Ni_3S_2 in Alkaline Medium. *Adv. Energy Mater.* **2018**, *8* (19), 1703538.